Journal of Naval Architecture and Marine Engineering
July, 2025
http://dx.doi.org/10.3329/jname.v22i2.76194 *http://www.banglajol.info*

HEAT SOURCE AND RADIATIVE MHD UPPER-CONVECTED MAXWELL NANOFLUID FLOW OVER AN INCLINED STRETCHING SHEET WITH CHEMICAL REACTION AND MULTI SLIP EFFECTS

Pennelli Saila Kumari[1], Shaik Mohammed Ibrahim[2]*

[1]Research Scholar, Department of Mathematics, Koneru Lakshmaiah Education Foundation, Green Fields, Vaddeswaram, Andhra Pradesh – 522302, India. Email address: mellacheruvu.saila@gmail.com.

[2*]Department of Mathematics, Koneru Lakshmaiah Education Foundation, Green Fields, Vaddeswaram, Andhra Pradesh. – 522302, India. Email address: ibrahimsvu@gmail.com.

Abstract:

The foremost empirical of this study is to research the flow of an Upper-Convected Maxwell (UCM) fluid including nanoparticles over an elongating surface on an inclined plane. The model analyzes the impression of an external magnetic field and investigates the impacts of linear thermal radiation, a heat source, and chemical processes under various slip situations. The Homotopy Analysis Method (HAM) is employed in order to work out the nonlinear equations that regulate the system through the provision of a robust framework for the accuracy of the solution. The principal findings are displayed in tabular and graphical formats. The findings indicate that an augmentation in magnetic field strength diminishes velocity profiles while enhancing both concentration as well as temperature profiles. Moreover, as the momentum slip consideration escalates, local Sherwood number and the local Nusselt number are diminish. The innovative discoveries are validated by comparisons with previous experimental and theoretical results, demonstrating practical applications in optimizing cooling systems, improving industrial heat exchangers, and increasing biotechnological processes such as wastewater treatment and pharmaceutical manufacture. Nanofluids and non-Newtonian fluids are being portrayed as highly effective solutions for next-generation cooling technologies as a result of this research, which provided a key insight into optimizing thermal management systems for advanced engineering applications.

Keywords: Inclined stretching sheet, chemical reaction, nanofluid, upper-convected Maxwell fluid, MHD, Multi slip effects.

Nomenclature:

U_∞	Free stream velocity	A	Momentum ratio significator
u, v	Velocities in (x, y) directions	Re_x	Local Reynolds number
B_0	intensity of magnetic field	Nu_x	Local Nusselt number
Le	Lewis number	κ	Thermal conductivity of fluid
U_∞	Free stream velocity	D_T	Thermophoresis diffusion coefficient
D_B	Random diffusion coefficient	Sh_x	Local Sherwood number
C	Volumetric Volume expansion coefficient	T_f	Thermal of a hot fluid
C_w	Uniform Concentration over the surface of the sheet	T_∞	ambient fluid thermal
C_∞	ambient concentration	Pr	Prandtl number
Nb	Random motion significator	R	Heat source parameter
Nt	Thermophoresis significator	f	Dimension less velocity stream function
S	Suction parameter	g	gravitational acceleration

 Received on: Sept., 2024

h_f	Heat transfer coefficient	R	Thermal radiation parameter
μ_∞	Limiting viscosity at infinite shear rate	$(\rho c)_f$	fluid heat capacity
h_f	Heat transfer coefficient	Γ	Solutal slip parameter
	Greek symbols	λ	Velocity slip parameter
μ	Dynamic viscosity of the fluid	δ_1	Velocity slip parameter
σ	electrical conductivity	δ_2	Thermal slip parameter
k^*	absorption coefficient	Q	Heat generation coefficient
η	dimensionless similarity variable	υ	kinematic viscosity of the fluid
χ_n	Characteristic function	Ω	Inclined sheet angle
Gr	Local Grashof number due to thermal	ξ	Relaxation time significator of the fluid
σ^*	Stefan -Boltzmann constant	ϕ_∞	Dimensionless solutal function at the surface

1. Introduction

The procedures of heat and mass transfer are extremely important in the fields of engineering and research. These processes have an effect on a broad variety of systems, ranging from industrial to biological applications. The effectiveness and efficiency of these processes are extremely important in a variety of technologies, such as cooling systems, chemical reactors, and medicinal equipment, amongst others. Research on heat and mass transmission has traditionally concentrated mostly on those fluids that are considered to be classical. Nanofluids, on the other hand, are colloidal suspensions of nanoparticles in base fluids. These nanofluids were developed as a result of breakthroughs in nanotechnology.

Because of their superior thermal properties in assessment to those of ordinary fluids, nanofluids have been the subject of intense research during the past few decades. The inclusion of nanoparticles causes a large increase in the thermal conductivity, viscosity, and convective heat transfer factors of these fluids, which ultimately leads to a major improvement in the thermal behavior of the fluids. This improvement can be due to a number of variables, including Random motion, thermophoresis, and the high surface area-to-volume ratio of nanoparticles. As a consequence of this, nanofluids are utilized in a variety of fields, including medical therapies, automotive systems, and electronic cooling.

Choi, and Eastman (1995) were the first to demonstrate that the incorporation of nanoparticles into nanofluids results in an increase in the thermal conductivity of base fluids. A significant amount of study and a great number of applications in a extensive variety of fields have been inspired by this breakthrough. Nanofluids have increased features that make them extremely favorable for a variety of engineering applications. These applications include computing, healthcare technology, power plant cooling, and automotive systems.

Microchip cooling, drug administration at the nanoscale, cancer treatment, cell preservation at low temperatures, and cryosurgery are only some of the applications that make use of nanofluids. Other uses include industrial cooling, nuclear reactors, geothermal energy extraction, automotive coolants, gasoline and brake fluids, and cryosurgery. Nanofluids are recognized as a highly valuable subject for research due to the specific properties that they possess. Additional research on nanofluids has been carried out by a number of researchers, including Reddy and Lakshminarayana (2022), Vinod Kumar Reddy et al. (2023), Madhu Kishan (2015), Madhu Kishan (2017), Meenakumari et al. (2023), and Macha, Naikoti et al. (2016), amongst others. Additional insights into this fascinating field of research are also provided by Reddy et al. (2024).

Non-Newtonian fluid concepts have been the topics of numerous investigations and theoretical research due to the vast range of biological and industrial procedures to which they are relevant. Numerous applications in industry, that include mixing, friction, energy slurries, biological fluids in cells and polymers, and pharmaceutical fluid, take non-Newtonian fluids into account as opposed to Newtonian fluid theory. When a

liquid moves through a medium, the rheology of the fluid is an important component that plays a role in determining the path that the liquid takes. The relationship between shear stress and shear rate provides the basis for the Newtonian and non-Newtonian kinds of fluid rheology, which are roughly classified into two major categories. Regardless of the shear rate that is applied, Newtonian fluids maintain a viscosity that is constant, but non-Newtonian fluids do not display this property. Researchers have demonstrated a strong interest in the study of the flow dynamics, as well as the transfer of heat and mass, of non-Newtonian fluids in a variety of geometries, taking into consideration a number of different factors. This interest is a direct result of the broad application of non-Newtonian fluids in a variety of applications, including industrial, medicinal, and food processing settings. Because the simplified Navier-Stokes equations are unable to effectively represent these fluids, it is necessary to build a variety of models in order to investigate their behavior.

Magnetohydrodynamics, also known as MHD, is a multidisciplinary field that combines concepts from magnetization and fluid physics in order to investigate the properties of electrically charged fluids. These fluids include plasmas, fluid metals, and seawater. The flow of magnetically charged fluids that is controlled by magnetic fields (MFs) is referred to as magnetically hardened fluid movement (MHD movement). Researchers Reddy et al. (2018b), Babu and Sandeep (2016), and Vijayalakshmi et al. (2017) have investigated the parameters that influence the flow of non-Newtonian fluids over a collection of stretched surfaces. Tian et al. (2018) conducted research on related phenomena, whereas Nasir et al. (2018) explored the effects of thermal radiation on magnetohydrodynamic three-dimensional flow over an extended surface. Both of these studies were published in 2018. Furthermore, Khan et al. (2018) examined the Eyring-Powell slip flow of a thin fluid layer containing graphene nanoparticles."

The Upper-Convected Maxwell (UCM) fluid is a viscoelastic, rate-type fluid model that takes into consideration the impacts of relaxation time while ignoring the complex influences of shear-dependent viscosity. This model provides a better understanding of the fluid's behavior. Numerous researchers, such as Imran et al. (2018), Yu Bai et al. (2017), Elbashbeshy et al. (2018), Vajravelu et al. (2017), Omowaye and Animasaun (2016), Alireza Rahbari et al. (2018), Gireesha et al. (2018), and Meysam Mohamadali and Ashrafi (2016), have conducted extensive research and brought attention to the significance of this model with their findings.

Earlier research conducted by Fetecau (2003) offered a precise solution for the movement of Maxwell fluids. While Wang and Hayat et al. (2008) researched the flow of Maxwell fluids in porous media, Fetecau et al. (2009) investigated the behavior of fractional Maxwell fluids in dynamic flows. Both of these studies were funded by the National Science Foundation. In Hayat et al. (2009) investigated two-dimensional Maxwell fluids that possessed magnetohydrodynamic (MHD) features. Heyhat and Khabzi (2011) conducted an investigation into the flow of MHD UCM fluids over surfaces that were rigid and flat. Furthermore, Hayat and Qasim (2010) established consecutive solutions for two-dimensional mesoscopic hydrodynamic flows that included thermophoresis. According to the findings of their investigation of non-Newtonian Maxwell fluids under a variety of different physical conditions, an upsurge in the Prandtl number results in a declination in the rates of temperature and heat transfer. Conditions such as viscous dissipation, Newtonian heating, chemical interactions, and temperature layers were taken into consideration in the studies, which were conducted across a variety of stretching surfaces.

The investigation of nanofluid flow at a stagnation point over an extended surface has a wide range of applications that can be found in a variety of technological sectors and industries. As a consequence of this, a great number of researchers have investigated this realm. The researchers Sajid et al. (2015), Srinivasulu et al. (2017), and Wubshet Ibrahim (2016) scrutinized magnetohydrodynamic (MHD) stagnation point flow in a variety of non-Newtonian fluids, including Oldroyd-B fluid, Casson fluid, and Upper-Convected Maxwell (UCM) fluid, on a stretching surface while taking into consideration a number of different physical parameters. In a similar manner, Mageswari and Nirmala (2016) investigated the flow at the stagnation point on an extended surface while Newtonian heating was present. In addition, Abuzar Ghaffari and colleagues (2017) investigated the impact of radiation and convective boundary conditions at the oblique stagnation point of non-Newtonian nanofluids that were flowing across an extended surface.

Stretching sheet metal in manufacturing entails using force to distort the material into a desired shape. The material flow is critical in this procedure. Stretching sheet metal includes plastic deformation, which causes the material to take on a shape permanently. The investigation of chemical reactions and slip boundary conditions in heat transfer is of great importance in a variety of applications, including those in the industries of technology and industry. The impacts of chemical processes on mass and heat transfer in magnetohydrodynamic (MHD)

boundary layer flow across a stretching sheet were explored by Mabood et al. (2016) and Ibrahim et al. (2017). These researchers took into consideration a variety of parameters, including viscous dissipation, thermal radiation, and mixed convection. The results of their investigation showed that the Nusselt number, the skin friction coefficient, and the Sherwood number all increased in proportion to the amount of intensity of themagnetic field.

Further investigation into the impact of slip conditions, viscous dissipation, and chemical processes on the MHD stagnation-point flow of nanofluids was carried out by Ibrahim and Negera (2020). The researchers made the observation that a drop in momentum occurs when the suction parameter is set to greater values. Studies on the effects of slip circumstances and chemical interactions may be found in the works of Ramzan and Bibal (2016) and Ramzan, Ullah et al. (2017). Both of these authors have published additional research on the subject.

According to the aforementioned body of research, a great number of studies have investigated the flow of fluid across a stretched sheet at a point of stagnation. The novelty of this research consists in the investigation of the fluid flow behavior under the influence of multi-slip effects on a non-Newtonian Upper-Convected Maxwell (UCM) fluid with nanofluid particles, combining Random motion and thermophoresis. This paper was inspired by the works that have been discussed previously. By investigating the effects of chemical reactions, heat sources, and thermal radiation, this study provides a fresh viewpoint on the ways in which these elements interact with one another to influence heat transfer and flow characteristics. As a result, our comprehension of energy efficiency and thermal regulation in advanced engineering applications may be improved. With the stretched sheet positioned on an inclined plane, the study investigates the combined impacts of parameters such as magnetohydrodynamics (MHD), temperature radiation, and chemical processes on flow, heat, and mass transfer in non-Newtonian nanofluids. Specifically, the paper focuses on the effects of these constraints on flow, heat, and mass transfer. To obtain solutions of the recent model, the homotopy analysis method (HAM) is employed, a semi-analytical technique successfully used. Implemented HAM to solve unsteady axisymmetric dynamics over time-dependent a radially stretching sheet and compare to results with a numerical method. This work not only advances the understanding of Casson hybrid nanofluid behaviour under various conditions but also contributes valuable insights for optimizing heat transfer systems in practical applications, aligning with the growing body of research that seeks to enhance thermal conductivity and heat transfer in nanofluid systems. This concept has the potential to be implemented in industrial heat exchangers in order to enhance heat dispersion by allowing the mixing of fluids using a variety of substances. Furthermore, the model has the potential to function as a cooling mechanism, which can help prevent medical equipment that is utilized for image processing from becoming overheated.

1.1 Motivation

Using multi-slip effects on an inclined stretched sheet, this study examines MHD non-Newtonian nanofluid flows, containing, chemical,species, and,heat,radiation. .We take into account the non-Newtonian behavior of the higher convected Maxwell fluid. Not only does this complex interaction lead to a deeper understanding of fundamental biological processes, but it also opens the door to new methods of diagnosis and treatment.

- Magnetohydrodynamics (MHD) is an exciting new approach that uses magnetic fields to precisely target disease areas with drug-carrying particles. This enables precision therapy without harming healthy cells.
- Although radiation effects are seldom associated with drug delivery, they can be a component of treatments like photodynamic therapy. This method activates light-sensitive medications using certain light wavelengths to produce a therapeutic effect, including the killing of cancer cells. To better understand the circulation-based delivery and activation of light-sensitive drugs, the model's inclusion of radiation consequences could be broadened.

1.2 Research questions

- How do thermal radiation and heat source influence the boundary layer flow and features of thermal transmission of UCM nanofluid?
- What is the impact of Brownian motions and thermophoresis's on the flow, thermal, and concentration profiles of UCM nanofluid in the presence of multiple slip effects?
- In what ways can magnetohydrodynamics (MHD) enhance or reduce the efficiency of heat transfer in UCM nanofluid?

- How can the HAM technique solver be utilized effectively to predict the implication of UCM fluid factors on thermal and flow distributions?
- What is the role of Schmidt number and Prandtl number in optimizing heat transfer and flow dynamics in a UCM nanofluid system?

2. Mathematical Formulation

In this study time-independent and incompressible MHD slip-up flow of upper-convected Maxwell (UCM) fluid sideways a elongating plane with chemical reaction which is sloping at an angle Ω from its upright axis. The x- and y- axes are connected along the sloping outward and regular to the surface as represented in Fig. 1. Here, spreading and free stream momentums are speculated as $u_w = ax,\ a > 0$ along the x-axis and $u_\infty = bx,\ b > 0$ *as* $y \to \infty$. The fluid is subjected to a magnetic field of intensity B_0 that is normal to the flow when the flow analysis is being done. The heat at the outward and afar gone the outward are indicated as T_w and T_∞ in that order, while concentration C_W and C_∞ also respectively.

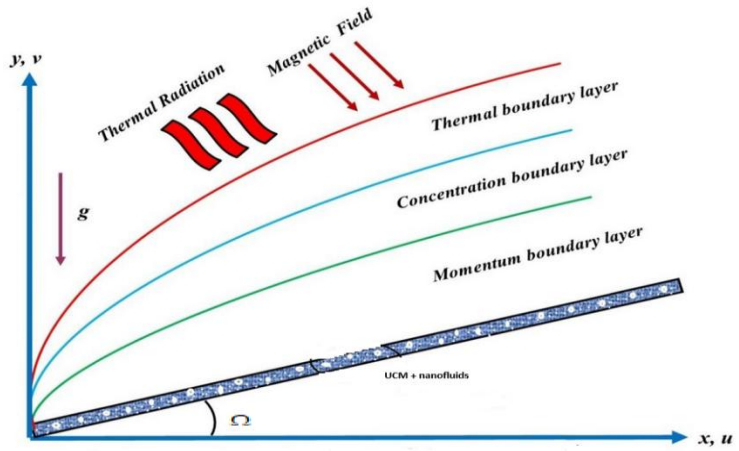

Fig. 1: Flow Model

Equations that incorporate the conversation laws of mass, momentum, energy, and concentration are included in the governing partial differential equations (PDEs) that characterize the motion of the UCM nanofluid, heat transfer, and mass transfer under the given assumptions. (Ibrahim and Negera (2020))

$$\frac{\partial u}{\partial x} + \frac{\partial v}{\partial y} = 0, \tag{1}$$

$$u\frac{\partial u}{\partial x} + v\frac{\partial u}{\partial y} = \upsilon\frac{\partial^2 u}{\partial y^2} - \xi\left(u^2\frac{\partial^2 u}{\partial x^2} + v^2\frac{\partial^2 u}{\partial y^2} + 2uvv\frac{\partial^2 u}{\partial x\,\partial y}\right) + g\left[\beta_T\left(T - T_\infty\right) + \beta_C\left(C - C_\infty\right)\right]\cos\Omega + U_\infty\frac{dU_\infty}{dx} + \frac{\sigma_f B^2(x)}{\rho_f}\left(U_\infty - u\right), \tag{2}$$

$$u\frac{\partial T}{\partial x} + v\frac{\partial T}{\partial y} = \alpha\frac{\partial^2 T}{\partial y^2} + \tau\left[D_B\frac{\partial C}{\partial y}\frac{\partial T}{\partial y} + \frac{D_T}{T_\infty}\left(\frac{\partial T}{\partial y}\right)^2\right] + \frac{Q_0}{(\rho c)_f}\left(T - T_\infty\right) - \frac{1}{(\rho c)_f}\frac{\partial q_r}{\partial y}, \tag{3}$$

$$u\frac{\partial C}{\partial x} + v\frac{\partial C}{\partial y} = D_B\frac{\partial^2 C}{\partial y^2} + \frac{D_T}{T_\infty}\frac{\partial^2 T}{\partial y^2} - Kr\left(C - C_\infty\right). \tag{4}$$

In accordance with the research conducted by Ibrahim and Negera (2020), the boundary conditions must be defined as

$$u = U_w(x) + \delta_1^*\left(\frac{\partial u}{\partial y}\right),\ v = V_w,\ T = T_w(x) + \delta_2^*\left(\frac{\partial T}{\partial y}\right),$$

$$C = C_w(x) + \delta_3^*\left(\frac{\partial C}{\partial y}\right) \text{ at } y = 0 \tag{5}$$

$$U \to U_\infty, \qquad T \to T_\infty,\ C \to C_\infty, \qquad \text{as} \qquad y \to \infty,$$

where $\alpha = \frac{k}{(\rho c)_f}$, $\upsilon = \frac{\mu}{\rho_f}$, $\tau = \frac{(\rho c)_p}{(\rho c)_f}$.

The nonlinear radiation is calculated by using the Rosseland approximation as follows:

$$q_r = -\frac{4\sigma^*}{3k^*}\left(\frac{\partial T^4}{\partial y}\right) = -\frac{16\sigma^* T^3}{3k^*}\frac{\partial T}{\partial y} \tag{6}$$

Moreover, the Taylor series is used to express the temperature T about the ambient temperature:

$$T^4 = T_\infty + 4(T - T_\infty)T_\infty^3 + 6(T - T_\infty)^2 T_\infty^2 + 4(T - T_\infty)^3 T_\infty + \ldots$$

When the higher-order terms are not included:

$$T^4 \approx -3\,T_\infty + 4(T - T_\infty)T_\infty^3 \tag{7}$$

Therefore, the linear radiation can be expressed as:

$$q_r = -\frac{4\sigma^*}{3k^*}\left(\frac{\partial T^4}{\partial y}\right) = -\frac{16\sigma^* T_\infty^{\ 3}}{3k^*}\frac{\partial T}{\partial y}$$

With above values the equation (3) transformed into

$$u\frac{\partial T}{\partial x} + v\frac{\partial T}{\partial y} = \left(\alpha + \frac{16\sigma^* T_\infty^3}{3\kappa^*(\rho c)_f}\right)\frac{\partial^2 T}{\partial y^2} + \tau\left[D_B\frac{\partial C}{\partial y}\frac{\partial T}{\partial y} + \frac{D_T}{T_\infty}\left(\frac{\partial T}{\partial y}\right)^2\right] + \frac{Q_0}{(\rho c)_f}(T - T_\infty), \tag{8}$$

It is possible to reduce the nonlinear PDEs to linear ODEs with the application of similarity transformations. The technique of similarity transformation related in this study is instructed as follows

$$\psi = (av)^{\frac{1}{2}} x f(\zeta), \theta(\zeta) = \frac{T - T_\infty}{T_W - T_\infty},\ \phi(\zeta) = \frac{C - C_\infty}{C_W - C_\infty},\ \zeta = \sqrt{\frac{a}{v}}y, \tag{9}$$

Here ζ is the similarity variable, Ψ is the stream function.

The stream function (ψ) now represents the momentum components in both x and y axis directions.

$$u = \frac{\partial \psi}{\partial y}, \qquad v = -\frac{\partial \psi}{\partial x} \tag{10}$$

This meets the continuity equivalence.

Similarity transformations are applied to convert the momentum, energy and mass equations into a nondimensional form.

$$f''' + ff'' + \delta\left(2ff'f'' - f^2 f'''\right) - f'^2 + \left(Gr\theta + Gc\phi\right)\cos\Omega + M\left(A - f'\right) + A^2 = 0, \tag{11}$$

$$\left(1 + \frac{4}{3}R\right)\theta'' + \Pr f\theta' + \Pr Nb\phi'\theta' + \Pr Nt\,\theta'^2 + \Pr Q\theta = 0, \tag{12}$$

$$\phi'' + Sc\left(f\phi' - \gamma\phi\right) + \frac{Nt}{Nb}\theta'' = 0. \tag{13}$$

The boundary conditions now transforms into

$$f(0) = S,\ f'(0) = 1 + \delta_1 f''(0), \theta(0) = \left(1 + \delta_2\theta'(0)\right),\ \phi(0) = \left(1 + \delta_3\phi'(0)\right),$$
$$f'(\infty) \to A, \theta(\infty) \to 0, \phi(\infty) \to 0, \tag{14}$$

where

$$\delta=\xi a,\quad M=\frac{\sigma_f B_0^2}{\rho_f a},\quad Gr_x=\frac{g\beta_T\left(T_w-T_\infty\right)x^3}{\upsilon^2},\quad Gr=\frac{Gr_x}{\mathrm{Re}_x^2},\quad Gc_x=\frac{g\beta_C\left(C_w-C_\infty\right)x^3}{\upsilon^2},\quad Gc=\frac{Gc_x}{\mathrm{Re}_x^2},$$

$$\mathrm{Re}_x=\frac{U_w x}{\upsilon}=\frac{ax^2}{\upsilon},\quad A=\frac{b}{a},\quad \mathrm{Pr}=\frac{\upsilon}{\alpha},\quad Nb=\frac{\tau D_B\left(C_w-C_\infty\right)}{\nu},\quad Nt=\frac{\tau D_T\left(T_w-T_\infty\right)}{\upsilon T_\infty},\quad R=\frac{4\sigma^* T_\infty^3}{k^* k},$$

$$Q=\frac{Q_0}{a\left(\rho c\right)_f},\ Sc=\frac{\upsilon}{D_B},\ \gamma=\frac{Kr}{a},\ \delta_1=\delta_1^*\sqrt{\frac{a}{\upsilon}},\ \delta_2=\delta_2^*\sqrt{\frac{a}{\upsilon}},\ \delta_3=\delta_3^*\sqrt{\frac{a}{\upsilon}},\ S=-\frac{V_w}{\sqrt{a\upsilon}}.$$

Non-dimensional skin friction coefficient C_f, Nusselt number Nu_x and Sherwood number Sh_x are

$C_f=\frac{\tau_w}{\rho U_w^2}$, $Nu_x=\frac{xq_w}{k\left(T_w-T_\infty\right)}$ and the Sherwood number $Sh_x=\frac{xq_m}{D_B\left(C_w-C_\infty\right)}$.,

Here τ_w q_w and q_m are the surface shear stress, heat flux and mass flux at the surface respectively given by

$$\tau_w=\mu\left(1+\delta\right)\left(\frac{\partial u}{\partial y}\right)_{y=0},\ q_w=\left(-\left(k+\frac{16\sigma^* T_\infty^3}{3k^*}\right)\left(\frac{\partial T}{\partial y}\right)\right)_{y=0},\ q_m=-\left(D_B\left(\frac{\partial u}{\partial y}\right)\right)_{y=0}.$$

Substituting q_w and q_m in the before equation, we get

$$\mathrm{Re}_x^{1/2}C_f=\left(1+\delta\right)f''(0),\ \mathrm{Re}_x^{-1/2}Nu_x=-\left(1+\frac{4R}{3}\right)\theta'\left(0\right)\text{ and }\mathrm{Re}_x^{-1/2}Sh_x=-\phi'\left(0\right).$$

3. Methodology for Solution

We devote the detailed initial approximations and linear operators to contain the homotopic methodologies to Equations (11) to (14). The following approach is illustrated in Fig. 2.

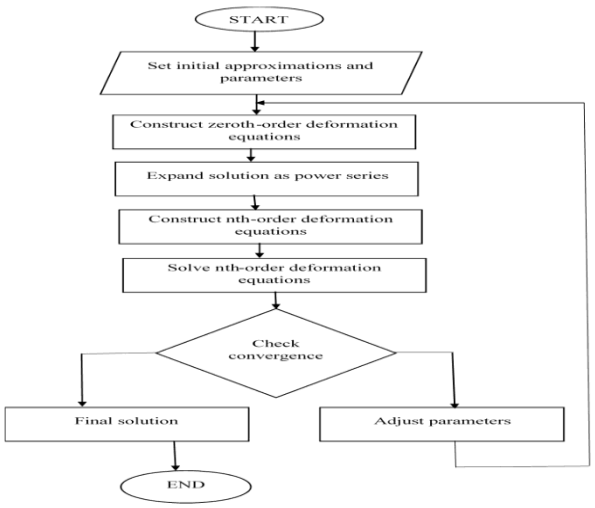

Fig. 2: Diagrammatic representation of HAM process.

It is demonstrated that the Homotopy Analysis Method (HAM), also known as the Homotopy Analysis Method, is an effective semi-analytical method by the fact that it is utilized in a variety of research projects to handle boundary layer flow issues. As an illustration, it has been successfully utilized to acquire semi-analytical solutions for the thermal convection boundary layer flow of incompressible Casson fluids. These solutions incorporate features such as suction/injection and heat sink effects, both of which are essential in polymer coating applications. In addition, the ability of HAM to handle non-linear boundary value problems has been demonstrated by the fact that it has been utilized to produce mathematical expressions for velocity, heat and mass transfer in boundary layer flows that involve thermal radiation in presence of multiple slip effects. The

approach has also been utilized in the field of magnetohydrodynamics, which has shed light on the impact that parameters like magnetic and Prandtl numbers have on flow characteristics. Additionally, the BVPh2.0 program has the capability to ease the implementation of HAM, which enables the efficient computing of solutions in complicated boundary layer situations that involve nanofluids and UCM fluids.

Employing the HAM allowed us to derive the analytic solutions for Eqs. (11)–(13) with the prescribed boundary conditions (14), using selected initial guesses and linear operators for the functions f, θ, and ϕ. In order to accomplish the development of the arrangement of ordinary differential equations, which is the basis for the formation of series solutions, the HAM technique was utilized. Linear operators L_{flow}, L_{temp} & L_{conc} and initial guesses f_O, θ_O & ϕ_O are taken in the form given following

$$f_O(\zeta) = S + A\zeta + \left(1 - e^{-\zeta}\right)\left(\frac{1-A}{1+\delta_1}\right),$$

$$\theta_O(\zeta) = \frac{e^{-\zeta}}{1+\delta_2},$$

$$\phi_O(\zeta) = \frac{e^{-\zeta}}{1+\delta_3},$$

$$L_{flow}(f) = f''' - f',$$

$$L_{temp}(\theta) = \theta'' - \theta,$$

$$L_{conc}(\phi) = \phi'' - \phi,$$

3.1 HAM convergence

Towards secure the apt ideals for the non-zero supporting considerations, $\hbar$ -bows are rendered in Fig. 2. As of this figure, the supposable interval of accessory constraint is $[-1.0, 0.0]$. The solutions are convergent for entire region of ζ when $\hbar_{flow} = \hbar_{temp} = \hbar_{conc} = -0.74$. Convergence of the technique is provided in Table. 1.

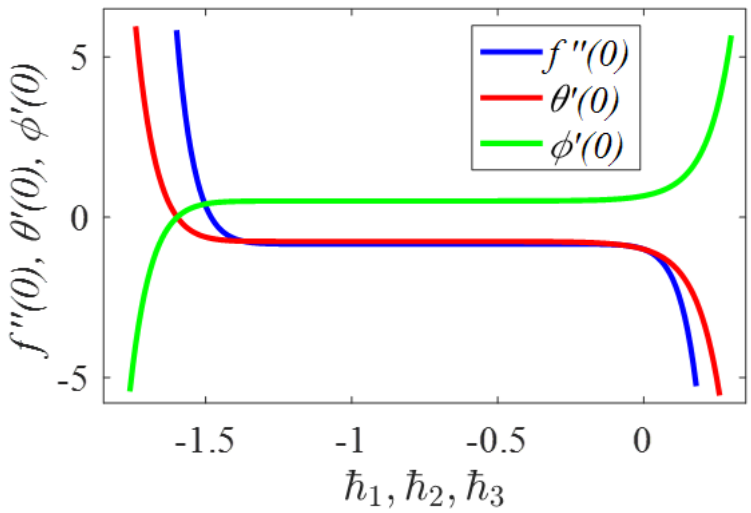

Fig. 3: $\hbar$ -curves of $f''(0)$, $\theta'(0)$ and $\phi'(0)$.

Table 1: Convergence of the HAM solution for different levels of approximation where
$Nb = 0.3, Nt = 0.2, \gamma = 0.2, \delta = R = S = A = \delta_1 = \delta_2 = \delta_3 = Q = Gr = Gc = 0.1, M = 0.5,$
$\Pr = Le = 2.0, \Omega = 60^o$

Order	$-f''(0)$	$-\theta'(0)$	$-\phi''(0)$
5	0.985462	0.715981	0.873952
10	0.921021	0.719778	0.871108
15	0.919537	0.719842	0.870952
20	0.919644	0.719843	0.870956
25	0.919632	0.719843	0.870956
30	0.919633	0.719843	0.870956
35	0.919633	0.719843	0.870956
40	0.919633	0.719843	0.870956

4. Results and Discussions

Within this subdivision, we demonstrated and studied the graphical implications that were produced as a result of the power series solution of the most significant ordinary differential equations (ODEs) problem to the borderline conditions that were given. Through the utilization of the Homotopy Analysis Method (HAM), this was successfully done. In order to examine the impact of an unlimited number of dimensionless constraints on the flow of a fluid, as well as heat and mass transfer profiles, the iterative power series solutions that are generated by HAM are applied. This approach is utilized in order to investigate the flow of a fluid. There are a number of parameters that are discussed graphically. These parameters include the Deborah number, suction/injection, velocity ratio constraint, radiation constraint, random motion, thermophoresis constraint, velocity slip, temperature slip, concentration slip parameter, magnetic parameter, chemical reaction, Lewis number, and microorganism profile. The temperature field, velocity profile, concentration profile, and microbe profile are all affected by these parameters in some way. In spite of the fact that the majority of the figures are created by iterating over a set of values for a specific significator, there are some figures that remain constant at a single value during the entirety of the simulation. These figures include:

$$Nb = 0.3, Nt = 0.2, \gamma = 0.2, \delta = R = S = A = \delta_1 = \delta_2 = \delta_3 = Q = Gr = Gc = 0.1, M = 0.5,$$
$$\Pr = Le = 2.0, \Omega = 60^o.$$

Table 1 presents a comparison of the variations in the skin coefficient, Sherwood, and Nusselt factors for numerous values of the *S, A,* δ_1 and δ, suction, velocity ratio, velocity slip and Deborah number relation to another study. The numbers indicate that our findings align commendably with those reported by researchers Ibrahim and Negera (2020) under limited conditions and we have reached a commendable consensus with him. Thus, we know that the numerical method is suitable for our problem analysis.

Table 1: Comparison among the mathematical evaluates of $-f''(0), -\theta'(0) \& -\phi'(0)$ for dissimilar values of S, A, δ_1 & δ when $Nb = Nt = R = Q = \gamma = \delta_2 = \delta_3 = 0.1, \Pr = Le = 2.0$.

S	A	δ_1	δ	Ibrahim and Negera (2020)			Present Outcomes		
				$-f''(0)$	$-\theta'(0)$	$-\phi'(0)$	$-f''(0)$	$-\theta'(0)$	$-\phi'(0)$
0.0	0.1	0.1	0.1	0.3215	0.6207	0.5638	0.321501	0.620549	0.563724
0.2				1.4387	0.8159	0.6097	1.438811	0.815872	0.609691
0.4				1.5730	1.0272	0.6530	1.572993	1.027315	0.653121
	0.2			1.2672	0.7441	0.6138	1.267198	0.744074	0.613799
	0.4			1.0091	0.7947	0.6619	1.009074	0.794653	0.661888
		0.2		1.3244	0.7069	0.5835	1.324413	0.706902	0.583512
		0.4		1.1418	0.6742	0.5703	1.141872	0.67164	0.570263
			0.2	1.4069	0.7111	0.5839	1.406910	0.711143	0.583548
			0.4	1.4647	0.7016	0.5776	1.464725	0.701672	0.577684

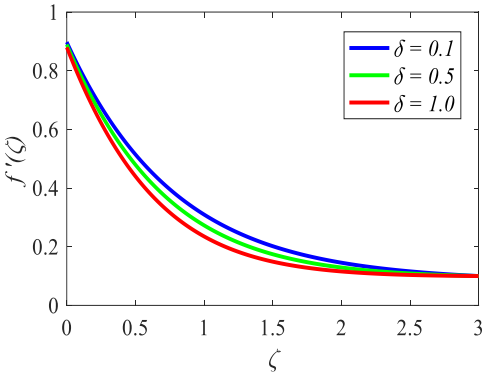

Fig. 4: Contours of $f'(\zeta)$ for δ.

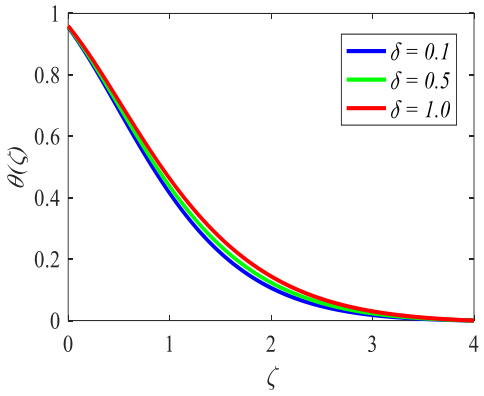

Fig. 5: Contours of $\theta(\zeta)$ for δ.

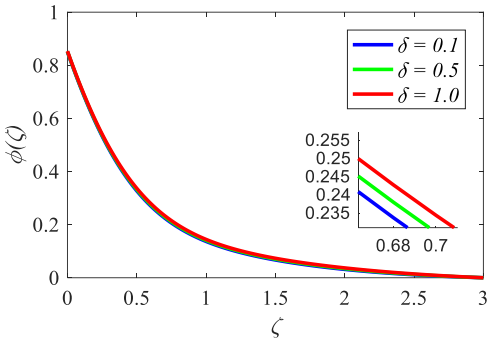

Fig. 6: Contours of $\phi(\zeta)$ for δ.

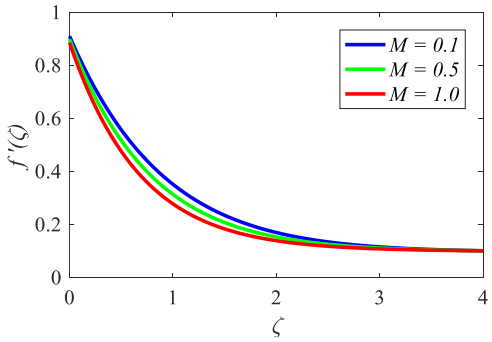

Fig. 7: Contours of $f'(\zeta)$ for M.

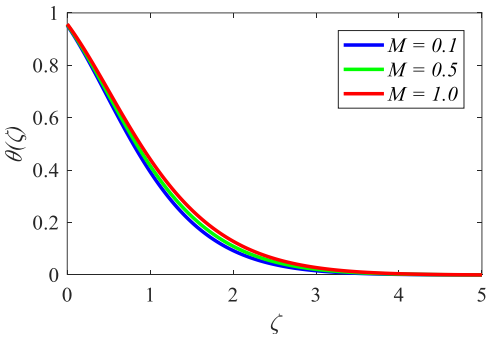

Fig. 8: Contours of $\theta(\zeta)$ for M

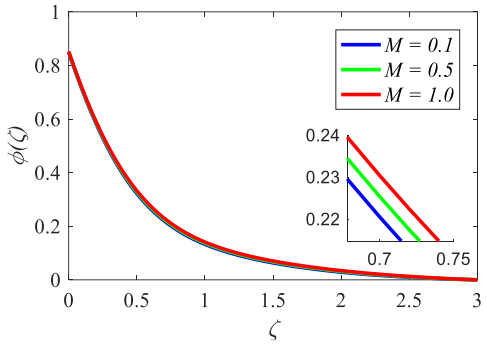

Fig. 9: Contours of $\phi(\zeta)$ for M

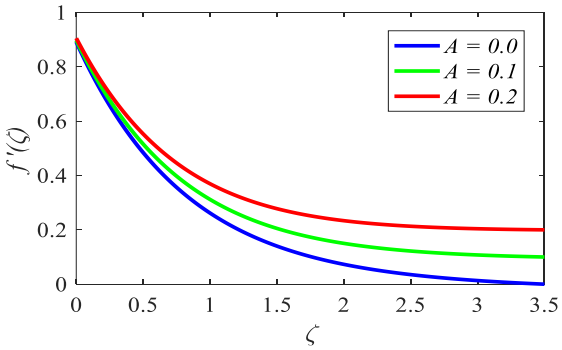

Fig. 10: Contours of $f'(\zeta)$ for A

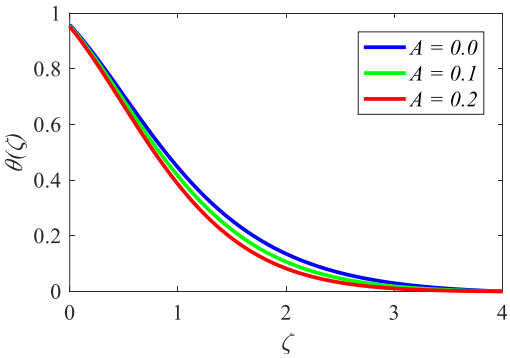

Fig 11: Contours of $\theta(\zeta)$ for A

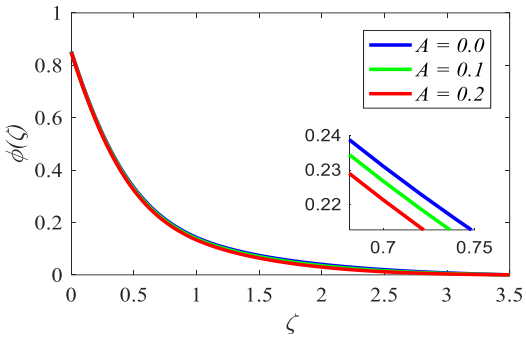

Fig. 12: Contours of $\phi(\zeta)$ for A

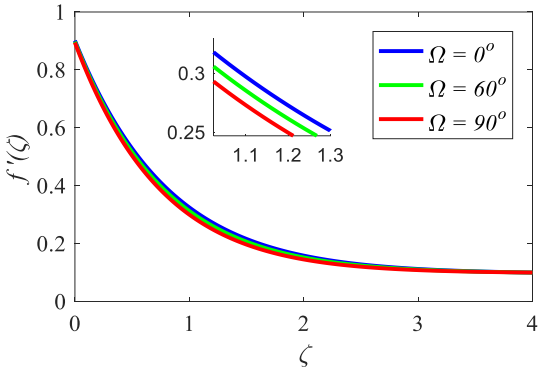

Fig. 13: Contours of $f'(\zeta)$ for Ω .

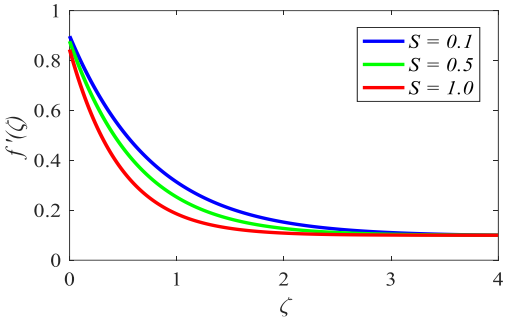

Fig. 14: Contours of $f'(\zeta)$ for S

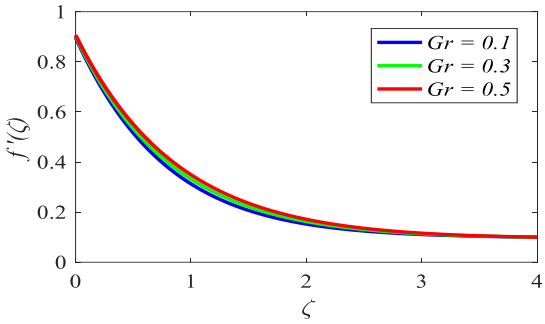

Fig. 15: Contours of $f'(\zeta)$ for Gr .

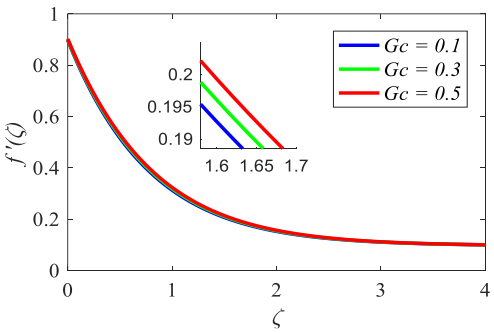

Fig. 16: Contours of $f'(\zeta)$ for Gc .

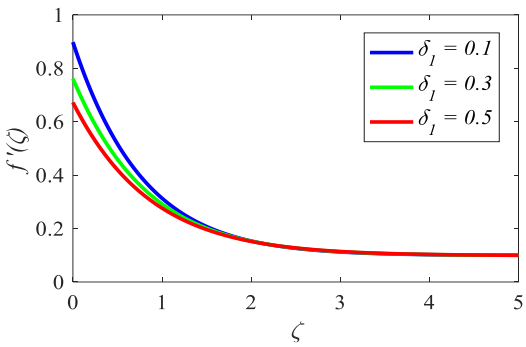

Fig. 17: Contours of $f'(\zeta)$ for δ_1

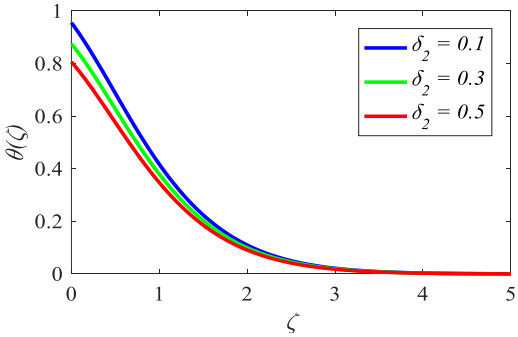

Fig. 18: Contours of $\theta(\zeta)$ for δ_2

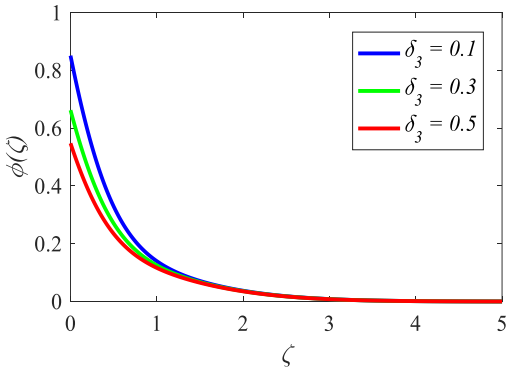

Fig. 19: Contours of $\phi(\zeta)$ for. δ_3.

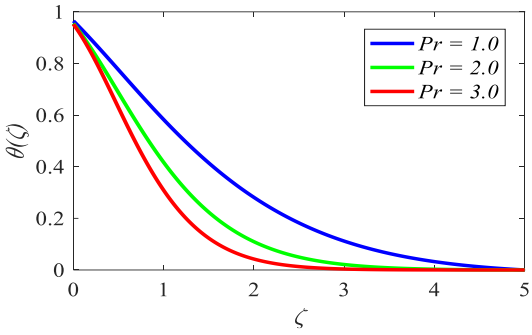

Fig. 20: Contours of $\theta(\zeta)$ for $\Pr$.

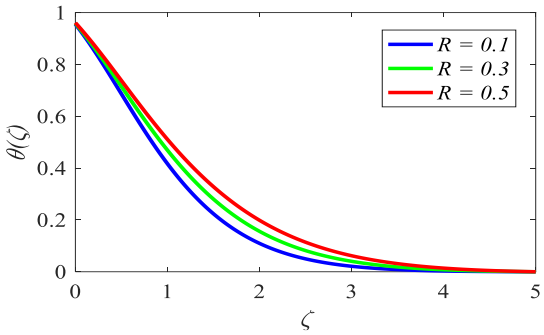

Fig. 21: Contours of $\theta(\zeta)$ for R.

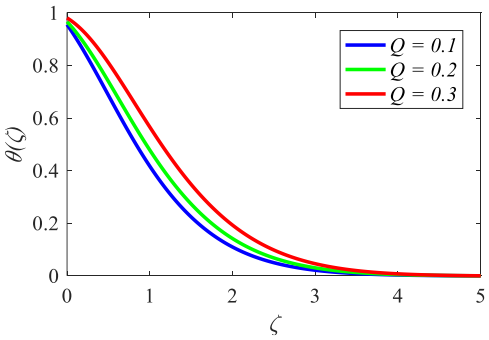

Fig. 22: Contours of $\theta(\zeta)$ for Q.

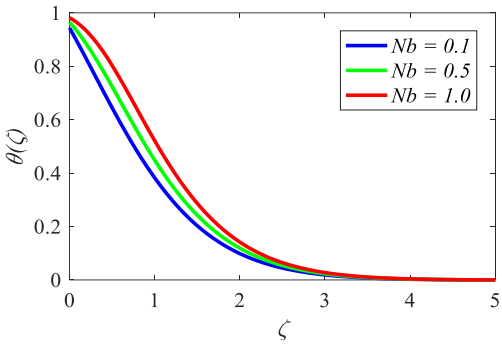

Fig. 23: Contours of $\theta(\zeta)$ for Nb.

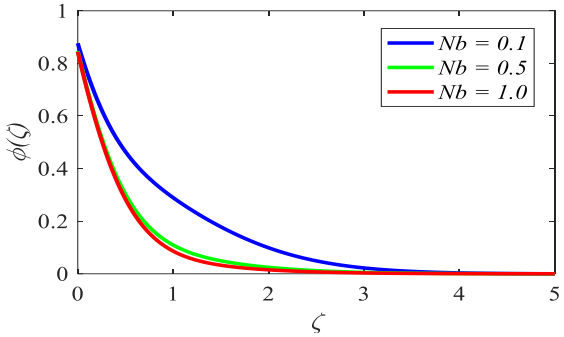

Fig. 24: Contours of $\phi(\zeta)$ for Nb.

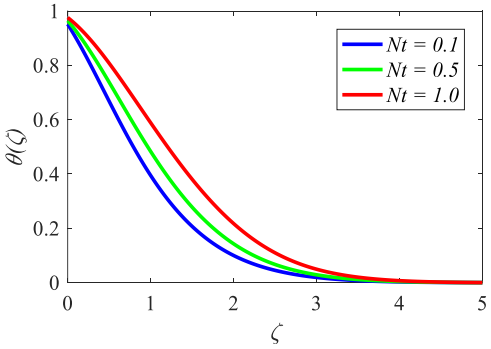

Fig. 25: Contours of $\theta(\zeta)$ for Nt.

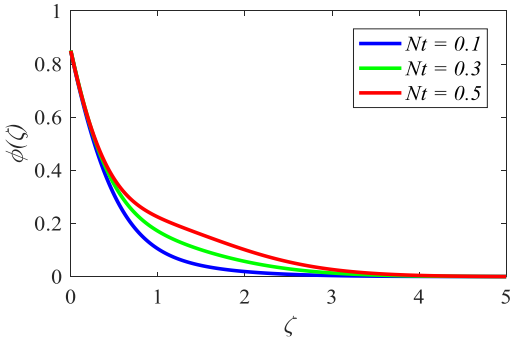

Fig. 26: Contours of $\phi(\zeta)$ for Nt.

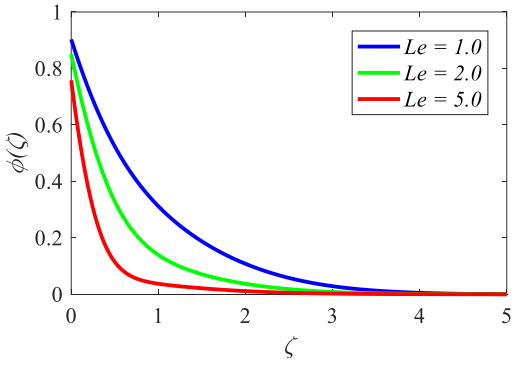

Fig. 27: Contours of $\phi(\zeta)$ for Le.

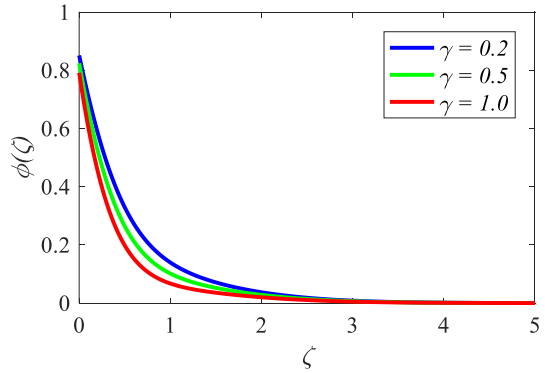

Fig. 28: Contours of $\phi(\zeta)$ for γ .

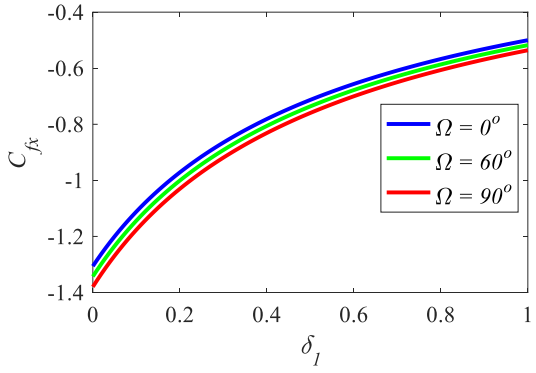

Fig. 29: Contours of Cf_x for Ω and δ_1 .

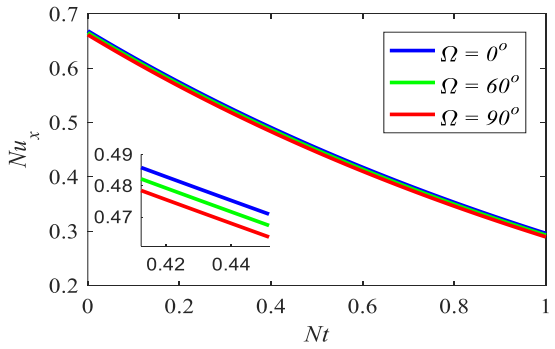

Fig. 30: Contours of Nu_x for Nt and Ω .

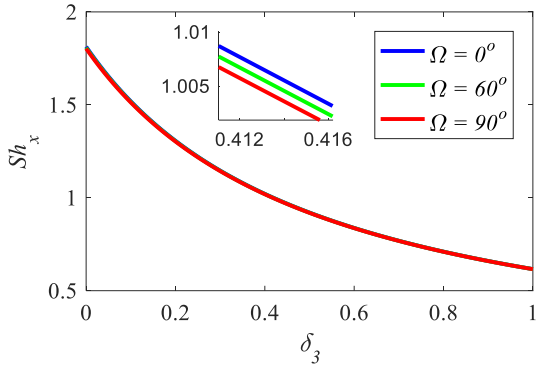

Fig. 3: Contours of Sh_x for Nt and Ω .

As seen in Figs. 2–4, the Deborah number has an effect on the profiles of Momentum, concentration, and thermal, respectively. These figures are presented in the order that they are shown. Based on the data that has been collected, it has been observed that the thickness of the boundary sheet for velocity decreases as the Deborah number increases. When the Deborah number is increased, on the other hand, the thicknesses of the thermal and solutal boundary layers increase as well. This is due to the fact that an increase in the Deborah number has the effect of producing forces that are in opposition to the flow of velocity. This is the reason why this effect occurs. Because of this, there is a decrease in the thermal diffusivity that occurs within the edge level, which ultimately leads to an increase in temperature.

Figs. 5, 6, and 7 illustrate, respectively, the impact that the magnetic field constraint has on the flow momentum, thermal contours, and solutal contours of the flow. The following numbers are shown in the order that was supplied. As the magnetic field increases, it is possible to observe that the momentum of the fluid decreases; yet, the temperature and solutal contours exhibit a tendency to increase. This can be observed in the photos. Additionally, the intensity of the magnetic field is increasing at the same moment. When the magnetic field is supplied to the system, a decelerating body force, which is also known as the Lorentz force, is introduced into the system. It is important to note that the direction in which this force acts is perpendicular to the direction in which the magnetic field is generated. The velocity boundary layer is reduced in length as a consequence of this force, which also results in a decrease in the thickness of the boundary layer.

Fig. 6 is a representation of the fluctuations that take place in the temperature profile. It also depicts the changes that take place in the magnetic parameter M. By increasing the magnetic limitation to higher levels, the temperature profile likewise increases accordingly. This is because the magnetic limitation is increasing. This is due to the fact that the application of a magnetic field to a conducting fluid causes the formation of a Lorentz force, which acts in opposition to the motion of the fluid, hence reducing the velocity of the fluid. As a consequence of this, a portion of the fluid's kinetic energy is converted into thermal energy as a result of the effects of resistive forces, which ultimately leads to an increase in temperature. This is the process that ultimately causes the temperature to rise. There is a tendency that can be seen in Fig. 7 that is comparable to the one that is seen in the concentration distribution.

Fig. 8 illustrates how the non-dimensional velocity contour evolves as the velocity ratio constraint A values are changed. This is shown in the figure. When the fluid goes further away from the wall, its velocity increases, but it decreases as it gets closer to the wall. This phenomenon occurs within the edge profiles. When the value of A is lower, it shows that the velocity of the wall is greater than the velocity of the free-stream. This is shown when the value of A is smaller. The momentum of the fluid initially drops as it approaches the wall because the inertia of the wall exerts an influence on the fluid at the boundary layer. This is because the wall has a different amount of inertia than the fluid. On the other hand, the fluid does experience a local acceleration at a specific distance from the wall, which may cause the local velocity to decrease below the velocity of the free stream. The slower-moving fluid is subsequently exhausted by the velocity of the free stream, which results in an increase in momentum. In Fig. 8, it is demonstrated that when A is equal to zero, the fluid does not experience the dragging effect of the free stream organization. In point of fact, the velocity of the free stream is very close to zero at this time. The local velocity that is external to the boundary film is rushed by the boring action of the free rivulet for all values of A that are greater than zero.

The variation in thermal contours that occurs as a result of a change in the values of velocity ratio significator A is illustrated in Fig. 9. The fact that the momentum ratio significator increases as the temperature boundary sheet thickness decreases is demonstrated by this. On top of that, the thermal at the surface increases (in absolute magnitude) as the momentum ratio significator increases. After all is said and done, the temperature summary decreases. The effect that momentum ratio significator A has on the solutal graph is depicted in Fig. 10 below. It is observed that the thickness of the solutal boundary layer decreases as the values of the momentum ratio significator increase. In addition, it is evident from the graph that the magnitude of heat on the surface of a plate increases as the momentum ratio significator increases.

Fig. 11 is a representation of the decreasing velocity profile that takes place when the parameter values increase, particularly with regard to the angle of inclination. The Lorentz forces cause the flow of the fluid to become more resistive, which in turn causes the velocity of the fluid to decrease. This leads to the fluid's velocity decreasing. The characteristic of the velocity profile in relation to the difference in the suction parameter S is depicted in Fig. 12, which may be found here. At the same time that the readings of the suction significator are increasing, the findings of the momentum contour are decreasing. Fig. 13 illustrates the properties of the local Grashof number (Gr), which can be found in the figure. This particular number has an impact on the shapes of the momentum. It will be possible to detect that the velocity profiles will also increase if the values of Gr are increased. This is something that can be observed. There is a representation of the effect that the concentration Grashof number (Gc) has on the velocity flow field that may be found in Fig. 14. The concentration Grashof number, often known as Gc, is a physical parameter that indicates the relative intensity of the species buoyant force in relation to the viscous hydrodynamic force in the boundary layer. Gc is an abbreviation for the concentration Grashof number. The results of an examination of the curves indicate that the concentration Grashof number (Gc) is the factor that is accountable for the acceleration of the momentum of the flow field at every location. The concentration buoyant force is increasing as a consequence of this particular reason, which is the reason for the increase.

As the velocity slip constraint δ_1 increases, the slip velocity experiences an increase while the fluid velocity experiences a reduction. This is due to the fact that the velocity of the stretching sheet and the stream are quite different when slip circumstances are present. The illustration of this phenomenon can be found in Fig. 15. A dissimilarity between the velocity of the stretching sheet and the momentum of the fluid stream near the sheet under slip conditions is responsible for the decrease in fluid velocity that occurs as the slip velocity increases. The illustration in Fig. 16 indicates that the temperature drops as the thermal slip δ_2 limitation is increased. The physical thickness of the thermal boundary layer is decreased when δ_2 is enlarged, which results in a reduction in the amount of heat that is transferred from the sheet to the fluid. With regard to the mass fraction field, the effect of the nanoparticle fraction slip constraint, δ_3, is comparable to the influence that it has on the temperature field, as demonstrated in Fig. 17. This similarity emerges due to the fact that slip impedes the mobility of fluids, which ultimately results in a reduction in the net transport of molecules. A drop in molecular activity leads to a declination in the mass fraction field, which is the result. Fig. 18 shows the thermal curves for various thermal radiation significator *R* values. It is evident from the graph that both the thermal graph and the thickness of the thermal boundary sheet rise as the values of the thermal radiation parameter do.

Fig. 19 The chart portrays that the thermal reduces when the Prandtl number Pr values of upsurges. This figure exposes that as an upsurge in Prandtl number Pr, the thermal field declines. A rise in the values of Pr decreases

the thermal diffusivity, because in the presence of (dimensionless number) Prandtl number which is termed as the ratio of momentum diffusivity to thermal diffusivity, that is Pr = ν/α. Growing the values of Pr implies that momentum diffusivity is more than thermal diffusivity. Therefore, temperature boundary sheet thickness is a declining function of Pr. In general, the Prandtl number is it also discloses that the solutal at surface of the plate rises.

A representation of Fig. 19 is provided for the purpose of examining the outcome of the heat generation/absorption significator on the thermal significator. The figure demonstrates that the thermal contour grows as the heat generation/absorption significator increases. This is something that can be noticed. This is due to the fact that the process of snowballing the formation of heat causes the temperature state of the fluid to increase. Figs. 20 and 21 illustrate how the Random motion parameter's influence can be seen in the contours of temperature and concentration. As the Random motion parameter grows, it is evident from these figures that the thermal gradient at the surface decreases, while at the same time, the thickness of the thermal boundary layer increases. On the other hand, the concentration contours and the thickness of the solutal boundary layer have a different impact, which is a decrease as the Random motion parameter is increased.

Fig. 22 and Fig. 23 illustrate the effect that the thermophoresis parameter has on the thermal contours and the solutal contours, respectively. These numerical values provide evidence that the thickness of the temperature boundary layer and the solutal boundary layer increases in a manner that is proportional to the thermophoresis parameter. An illustration of how the Lewis number influences solutal outlines can be found in Fig. 24. The solutal profile and the thickness of the solutal border layer are both reduced when the Lewis numbers are increased, as can be seen in the above image.

On the solutal field, the effect of the chemical reaction constraint γ is plotted in Fig. 25, which may be found here. A decrease in the solutal contour is observed when the values of the chemical reaction constraint are increased. Mainly due to the fact that a higher reaction rate results in a more rapid consumption of the reactive species involved. An increase in the reaction parameter causes the reaction to become more intense, which in turn causes the reactant to be depleted significantly more quickly. It is because of this that the concentration of the reactive species decreases at a faster rate, which ultimately results in a more precipitous decline in the concentration profile.

The skin-friction factor is displayed in Fig. 27, which illustrates the fluctuation of Ω and δ_1. Upon observation, it has been observed that the skin-friction coefficient increases as both Ω and δ_1 are increased. As shown in Fig. 29, it is observed that the Nusselt number drops as the limitations *Nt* and Ω are increased. Fig. 30 illustrates the rise in Sherwood number that occurs as a consequence of the fluid's high molecular diffusivity and poor heat conductivity at the same time. Examples of the δ_3 and Ω variances are presented here. As the values of δ_3 and Ω grow, the momentum of the fluid in the boundary layer falls in the vicinity of the wall.

Conclusions

The purpose of this study is to investigate the effects of MHD multi slide flow on an upper-convected Maxwell fluid (UCM) nanofluid that is flowing over an inclined elongating surface while chemical reactions are taking place. During the inspection, a number of different controlling factors are taken into consideration. These include the ratio of speeds, the parameter of suction-injection, the number of Lewis, the magnetic field, the parameter of Random motion, the significator of thermophoresis, the significator of chemical reaction, the significator of thermal radiation, the significator of velocity slip, the significator of temperature slip, the significator of concentration slip, and the significator of heat source. It is possible to arrive at a solution that is comparable by taking into consideration these parameters. The conclusions offer a detailed assessment of the findings of the most recent research as well as the ramifications of those findings, so highlighting the significance of the work that has been done in the field.

- As a result of the opposing Lorentz forces, increasing the magnetic parameter causes velocity profiles to be dampened across all nanofluids and now-Newtonian fluids. This results in flattened velocity distributions, while simultaneously improving temperature and concentration profiles through improved thermal mixing, particularly in UCM and nanofluid matrices.

- Random motion, thermophoresis, and Prandtl number all contribute to a decrease in temperature profiles, but there is a rise in temperature profiles when radiation parameters are raised.

- The drop in concentration profiles that occurs with increasing chemical reaction and Schmidt parameters is a consequence of the increased consumption of reactive species and the decreased mass diffusivity experienced.

- A high level of accuracy was demonstrated by the Homotopy Analysis Method (HAM) that was utilized in this investigation for the purpose of estimating the momentum and thermal contours of the nanofluids examined. Because of its adaptability in dealing with nonlinear differential equations, it enables precise modeling of complex fluid behaviors under a wide range of situations, which in turn strengthens the dependability of the results that are achieved.

- The findings highlight the possibility of employing nanofluids, particularly those that incorporate graphene oxide, for applications that need efficient heat transfer and flow dynamics. Some examples of these applications include cooling systems, thermal energy storage, and a variety of industrial processes.

- For the purpose of optimizing the performance of nanofluids in applications that take place in the real world, it is recommended that additional research be conducted into the impacts of other base fluids, varied concentrations of nanoparticles, and additional flow conditions.

Acknowledgements

We are grateful to the reviewers for their time, insightful remarks, and useful ideas, all of which contributed to the significant improvement of this work. We were able to improve the depth and clarity of our study by utilizing their knowledge and particular critiques.

References

Babu, M. J., & Sandeep, N. (2016): MHD non-Newtonian fluid flow over a slandering stretching sheet in the presence of cross-diffusion effects. Alexandria Engineering Journal, Vol. 55, No. 3, pp. 2193-01. https://doi.org/10.1016/j.aej.2016.06.009

Bai, Y., Jiang, Y., Liu, F., & Zhang, Y. (2017): Numerical analysis of fractional MHD Maxwell fluid with the effects of convection heat transfer condition and viscous dissipation. AIP Advances, Vol. 7, No.. 12. https://doi.org/10.1063/1.5055690

Bidin, B., & Nazar, R. (2009): Numerical solution of the boundary layer flow over an exponentially stretching sheet with thermal radiation. European journal of scientific research, Vol. 33, No. 4, pp. 710-17. http://www.eurojournals.com/ejsr.htm

Choi, S.U., Eastman, J.A.: Enhancing thermal conductivity of fluids with nanoparticles. Argonne National Lab.(ANL), Argonne, IL (United States) (1995). Conference: 1995 International mechanical engineering congress and exhibition, San Francisco, CA (United States), 12-17 Nov 1995; Other Information: PBD: Oct 1995

Elbashbeshy, E. M. A. R., Abdelgaber, K. M., & Asker, H. G. (2018): Heat and mass transfer of a Maxwell nanofluid over a stretching surface with variable thickness embedded in porous medium. International Journal of Mathematics and Computational Science, Vol. 4, No. 3, pp. 86-98. http://www.aiscience.org/journal/ijmcs

Fetecau, C., & Fetecau, C. (2003): A new exact solution for the flow of a Maxwell fluid past an infinite plate. International Journal of Non-Linear Mechanics, Vol. 38, No. 3, pp. 423-27. https://doi.org/10.1016/S0020-7462(01)00062-2

Fetecau, C., Athar, M., & Fetecau, C. (2009): Unsteady flow of a generalized Maxwell fluid with fractional derivative due to a constantly accelerating plate. Computers & Mathematics with Applications, Vol. 57, No. 4, pp. 596-603. https://doi.org/10.1016/j.camwa.2008.09.052

Ghaffari, A., Javed, T., & Labropulu, F. (2017): Oblique stagnation point flow of a non-Newtonian nanofluid over stretching surface with radiation: a numerical study. Thermal Science, Vol. 21, No. 5, pp. 2139-153. https://doi.org/10.2298/TSCI150411163

Gireesha, B. J., Mahanthesh, B., Gorla, R. S. R., & Krupalakshmi, K. L. (2018): Mixed convection two-phase flow of Maxwell fluid under the influence of non-linear thermal radiation, non-uniform heat source/sink and fluid-particle suspension. Ain Shams Engineering Journal, Vol. 9, No. 4, pp. 735-46. https://doi.org/10.1016/j.asej.2016.04.020

Hayat, T., Abbas, Z., & Sajid, M. (2009): MHD stagnation-point flow of an upper-convected Maxwell fluid over a stretching surface. Chaos, Solitons & Fractals, Vol. 39, No. 2, pp. 840-48. https://doi.org/10.1016/j.chaos.2007.01.067

Hayat, T., & Qasim, M. (2010): Influence of thermal radiation and Joule heating on MHD flow of a Maxwell fluid in the presence of thermophoresis. International Journal of Heat and Mass Transfer, Vol. 53, No. (21-22), pp. 4780-4788 https://doi.org/10.1016/j.ijheatmasstransfer.2010.06.014

Heyhat, M. M., & Khabazi, N. (2011): Non-isothermal flow of Maxwell fluids above fixed flat plates under the influence of a transverse magnetic field. Proceedings of the Institution of Mechanical Engineers, Part C: Journal of Mechanical Engineering Science, Vol. 225, No. 4, pp. 909-16. https://doi.org/10.1243/09544062JMES2245

Imran, M. A., Riaz, M. B., Shah, N. A., & Zafar, A. A. (2018): Boundary layer flow of MHD generalized Maxwell fluid over an exponentially accelerated infinite vertical surface with slip and Newtonian heating at the boundary. Results in physics, Vol. 8, pp. 1061-1067. https://doi.org/10.1016/j.rinp.2018.01.036

Ibrahim, S. M., Lorenzini, G., Kumar, P. V., & Raju, C. S. K. (2017): Influence of chemical reaction and heat source on dissipative MHD mixed convection flow of a Casson nanofluid over a nonlinear permeable stretching sheet. International Journal of Heat and Mass Transfer, Vol. 111, pp. 346-55. https://doi.org/10.1016/j.ijheatmasstransfer.2017.03.097

Ibrahim, W. (2016): Magnetohydrodynamic (MHD) stagnation point flow and heat transfer of upper-convected Maxwell fluid past a stretching sheet in the presence of nanoparticles with convective heating. Frontiers in Heat and Mass Transfer , Vol. 7, No. 1,. https://doi.org/10.5098/hmt.7.4

Ibrahim, W., & Negera, M. (2020): MHD slip flow of upper-convected Maxwell nanofluid over a stretching sheet with chemical reaction. Journal of the Egyptian Mathematical Society, Vol. 28, No. 1, pp. 21-32.. https://doi.org/10.1186/s42787-019-0057-2

Khan, N. S., Zuhra, S., Shah, Z., Bonyah, E., Khan, W., & Islam, S. (2018): Slip flow of Eyring-Powell nanoliquid film containing graphene nanoparticles. AIP Advances, Vol. 8, No. 11, pp. 212-24.. https://doi.org/10.1063/1.5055690

Lu, D. C., Ramzan, M., Bilal, M., Chung, J. D., & Farooq, U. (2018): A numerical investigation of 3D MHD rotating flow with binary chemical reaction, activation energy and non-Fourier heat flux. Communications in Theoretical Physics, Vol. 70, No. 1, pp. 89-99. DOI 10.1088/0253-6102/70/1/89

Macha, M., Naikoti, K., & Chamkha, A. J. (2016): MHD flow of a non-Newtonian nanofluid over a non-linearly stretching sheet in the presence of thermal radiation with heat source/sink. Engineering Computations, Vol. 33, No. 5, pp. 1610-26. https://doi.org/10.1108/EC-06-2015-0174

Madhu, M., Kishan, N., & Chamkha, A. J. (2017b): Unsteady flow of a Maxwell nanofluid over a stretching surface in the presence of magnetohydrodynamic and thermal radiation effects. Propulsion and Power research, Vol. 6, No. 1, pp. 31-40. https://doi.org/10.1016/j.jppr.2017.01.002

Madhu, M., & Kishan, N. (2017): MHD flow and heat transfer of Casson nanofluid over a wedge. Mechanics & Industry, Vol. 18, No. 2, pp. 210-21. https://doi.org/10.1051/meca/2016030

Mohamadali, M., & Ashrafi, N. (2016). Similarity Solution for High Weissenberg Number Flow of Upper-Convected Maxwell Fluid on a Linearly Stretching Sheet. Journal of Engineering, Vol. 2016, No. 1, pp. 9718786 https://doi.org/10.1155/2016/9718786

Mageswari, M., & Nirmala, M. (2016): Stagnation point flow over a stretching sheet with Newtonian heating using Laplace domain decomposition method. International Journal of Pure and Applied Mathematics, Vol. 110, No. 1, pp. 95-102., doi: 10.12732/ijpam.v110i1.11.

Mabood, F., Shateyi, S., Rashidi, M. M., Momoniat, E., & Freidoonimehr, N. J. A. P. T. (2016): MHD stagnation point flow heat and mass transfer of nanofluids in porous medium with radiation, viscous dissipation and chemical reaction. Advanced Powder Technology, Vol. 27, No. 2, pp. 742-49. https://doi.org/10.1016/j.apt.2016.02.033

Meenakumari, R., Lakshminarayana, P., Vajravelu, K., & Sucharitha, G. (2023): Convective heat and mass transfer analysis on Casson nanofluid flow over an inclined permeable expanding surface with modified heat flux and activation energy. Numerical Heat Transfer, Part A: Applications, 1–20. https://doi.org/10.1080/10407782.2023.2275281

Nasir, S., Islam, S., Gul, T., Shah, Z., Khan, M. A., Khan, W., ... & Khan, S. (2018): Three-dimensional rotating flow of MHD single wall carbon nanotubes over a stretching sheet in presence of thermal radiation. Applied Nanoscience, Vol. 8, pp. 1361-78. . https://doi.org/10.1007/s13204-018-0766-0

Omowaye, A. J., & Animasaun, I. L. (2016): Upper-convected maxwell fluid flow with variable thermo-physical properties over a melting surface situated in hot environment subject to thermal stratification. Journal of applied fluid mechanics, Vol. 9, No. 4, pp. 1777-90. 10.18869/acadpub.jafm.68.235.24939

Rahbari, A.,Abbasi, M., Rahimipetroudi, I., Sundén, B., Domiri Ganji, D., & Gholami, M. (2018): Heat transfer and MHD flow of non-Newtonian Maxwell fluid through a parallel plate channel: analytical and numerical solution. Mechanical Sciences, Vol. 9, No. 1, pp.61-70. https://doi.org/10.5194/ms-9-61-2018

Ramzan, M., & Bilal, M. J. J. O. M. L. (2016): Three-dimensional flow of an elastico-viscous nanofluid with chemical reaction and magnetic field effects. Journal of Molecular Liquids, Vol. 215, pp. 212-20 https://doi.org/10.1016/j.molliq.2015.12.036

Reddy, M. V., & Lakshminarayana, P. (2022): MHD radiative flow of Williamson nanofluid with Cattaneo-Christov model over a stretching sheet through a porous medium in the presence of chemical reaction and suction/injection. Journal of Porous Media, Vol. 25, No. 12. https://doi.org/10.1615/JPorMedia.2022041423

Reddy, M. V., Meenakumari, R., Sucharitha, G., Ali, F., Zafar, S. S., & Lakshminarayana, P. (2024): Heat and mass transfer analysis of conducting non-Newtonian nanofluid flows over an elongating sheet with a non-uniform heat source. Modern Physics Letters B, 2450349. https://doi.org/10.1142/S0217984924503494

Ramzan, M., Ullah, N., Chung, J. D., Lu, D., & Farooq, U. (2017): Buoyancy effects on the radiative magneto Micropolar nanofluid flow with double stratification, activation energy and binary chemical reaction. Scientific reports, Vol. *7, No.* 1, pp. 12901. OI:10.1038/s41598-017-13140-

Reddy, J. R., Kumar, K. A., Sugunamma, V., & Sandeep, N. (2018): Effect of cross diffusion on MHD non-Newtonian fluids flow past a stretching sheet with non-uniform heat source/sink: A comparative study. Alexandria engineering journal, Vol. 57, No. 3, pp. 1829-38.. https://doi.org/10.1016/j.aej.2017.03.008

Sajid, M., Ahmed, B., & Abbas, Z. (2015): Steady mixed convection stagnation point flow of MHD Oldroyd-B fluid over a stretching sheet. Journal of the Egyptian Mathematical Society, Vol. 23, No. 2, pp. 440-44. https://doi.org/10.1016/j.joems.2014.05.013Get rights and content

Srinivasulu, T., Bandari, S., & Sumalatha, C. (2017): MHD stagnation point flow of Casson nanofluid over a stretching sheet with effect of viscous dissipation. Global Journal of Pure and Applied Mathematics, Vol 13, No. 8, pp. 4229-44. http://www.ripublication.com

Tian, X. Y., Li, B. W., & Hu, Z. M. (2018): Convective stagnation point flow of a MHD non-Newtonian nanofluid towards a stretching plate. International Journal of Heat and Mass Transfer, Vol. 127, pp. 768-80 https://doi.org/10.1016/j.ijheatmasstransfer.2018.07.033

Vajravelu, K., Li, R., Dewasurendra, M., Benarroch, J., Ossi, N., Zhang, Y., ... & Prasad, K. V. (2017):. Analysis of MHD boundary layer flow of an Upper-Convected Maxwell fluid with homogeneous-heterogeneous chemical reactions. Communications in Numerical Analysis, Vol. 2, pp. 202-16 doi:10.5899/2017/cna-00324

Vijayalakshmi, R., Sreelakshmi, K., Sandhya, G., & Sarojamma, G. (2017): Flow of upper-convected Maxwell Micropolar fluid over a stretching sheet with slip effect. International Journal of Innovative Research in Science, Vol. 6, No. 13, pp. 148-54.

Vinodkumar Reddy, M., Vajravelu, K., Lakshminarayana, P., & Sucharitha, G. (2023): Heat source and Joule heating effects on convective MHD stagnation point flow of Casson nanofluid through a porous medium with chemical reaction. Numerical Heat Transfer, Part B: Fundamentals, Vol. 85, No. 3, pp. 286–304. https://doi.org/10.1080/10407790.2023.2233694

Wang, Y., & Hayat, T. (2008): Fluctuating flow of a Maxwell fluid past a porous plate with variable suction. Nonlinear Analysis: Real World Applications, Vol. 9, No. 4, pp. 1269-82 https://doi.org/10.1016/j.nonrwa.2007.02.016